A digital tool to design structurally feasible semi-circular masonry arches composed of interlocking blocks

C. Casapulla[*1], E. Mousavian[1], M. Zarghani[2]

[1] *Department of Structures for Engineering and Architecture, University of Naples Federico II, via Forno Vecchio 36, 80134, Naples, Italy*

[2] *School of Civil Engineering, Iran University of Science and Technology, Tehran, Iran*

[*] *Corresponding author (Claudia Casapulla)*
Tel./fax: +39 081 2538901
E-mail: casacla@unina.it

Abstract. *This work deals with a digital tool to design stable semi-circular masonry arches composed of interlocking blocks which are kept together by interlocking connectors on their faces. These blocks, comparing to conventional blocks, increase the sliding resistance and reduce the workmanship. However, the digital tools were developed mostly to design arches with conventional blocks. The proposed tool tries to fill this gap by addressing the work in three stages.*

First, a heuristic method is developed to define the relationships between the geometry of an interlocking face and the sliding resistance. Then, a structural analysis procedure is developed based on the limit analysis and the heuristic method to define the stability condition of the arch. Finally, optimization algorithms are developed to find the thinnest arch by means of two minimization strategies dealing with the relationship between the sliding resistance of the blocks and the geometry of the interlocking faces, differently. The algorithms consider some control points on a given thrust line and automatically adjust them to minimize the thickness, while the stability condition checks the structural feasibility during the geometry adjustment. To evaluate the accuracy of the proposed heuristic method, the results obtained with nonlinear FE analysis are used for comparison.

Keywords: Structurally informed architectural design, digitally supported design, limit analysis, interlocking blocks, non-isotropic sliding resistances, thrust line.

Claudia Casapulla, Elham Mousavian, Mohsen Zarghani, A digital tool to design structurally feasible semi-circular masonry arches composed of interlocking blocks,

Computers & Structures, 221 (2019):111-126.

DOI: http://dx.doi.org/10.1016/j.compstruc.2019.05.001

1. INTRODUCTION

This work develops a digital tool to design structurally sound semi-circular masonry arches composed of interlocking blocks. The interlocking blocks are rigid block units which, on their faces, have connectors keeping the blocks together and preventing blocks from sliding. The interlocking blocks, in comparison to the conventional blocks with flat faces, increase the shear resistance to external forces [1] and reduce the construction skills and instruments required [2]. Despite these advantages of interlocking blocks, the digital tools supporting designers for structurally informed architectural design were developed mostly for the conventional blocks. Most of those efforts (reviewed by Rippmann [3]) were focused on designing single-layer masonry vaults. To design masonry assemblages with diverse topologies, Whiting [4] proposed a method in which, given a block assemblage, the block geometry changes automatically to obtain the structurally feasible form. In that work, however, interlocking the blocks during the geometry modification was avoided. There are a few studies [5, 6] that applied simple geometric grammars but no structural constraints to design vaults that are composed of interlocking blocks with limited geometries.

In the literature there are different methods of structural analysis to develop the introduced digital tools. Most of them are based on the limit analysis theory aimed at calculating the ultimate load factor satisfying static and kinematic conditions. According to this theory, internal forces are distributed at the interfaces between rigid blocks. These interfaces have infinite compressive, no tensile strength, and infinite [7] or finite sliding resistance including associative [8, 9] or non-associative [10-13] frictional resistance. In this framework, it is worthy to mention a recent numerical limit analysis procedure, named discontinuity layout optimisation (DLO) [14], which has been developed to obtain accurate upper-bound solutions for plane-strain collapse problems. With reference to vaulted single-layered masonry structures, different methods find the stress states at interfaces: line of thrust methods [7, 15, 16]; membrane theory [7, 17, 18]; force network method [19, 20]; convex and concave contact formulations [9, 21], non-smooth contact dynamics [22]. Interesting are also some recent experimental and/or analytical works on the collapse failure of vaulted masonry structures under horizontal loading [23, 24] and after actual displacements of the supports [25-27]. However, all these methods were applied to analyze structures composed of conventional block with isotropic friction.

Other distinctive methods of masonry analysis, such as discrete and finite element analysis, rarely have been used to develop tools to design structurally feasible masonry assemblages,

mostly due to their complex computational techniques. In the former method, masonry is modelled as an assemblage of distinct blocks. For such a block system, the equations of motion are solved using an explicit time integration method [28-30]. Instead, in finite element analysis (FEA), masonry is modelled as connected or distinct elements with different material properties for bricks and mortar joints (detailed and simplified micro models) or as a continuum by smearing the bricks and mortar joints into an isotropic or anisotropic homogeneous continuum (macro models) [31-33].

This work aims at filling the gaps described above about design of structurally sound assemblages of interlocking blocks and proposes a digital framework for the structurally informed design of a semi-circular arch composed of interlocking blocks and subjected to its own weight. To develop this framework, limit state analysis is adopted and extended to interlocking blocks. This structural typology with symmetrical loading and geometry belongs to a special class of non-associative friction problems for which provably unique solutions within limit analysis approach exist [16]. Therefore, the application to this structure allows focusing the attention to the structural behaviour of interlocking blocks rather than to the issue of associated or non-associated flow rules, which is beyond the scope of this work.

Three main stages are herein introduced to help the designer to evaluate the structural feasibility of a model and automatically update the model to make it structurally optimal.

1. The first stage of this work is to develop a novel heuristic method, assisting the designers to estimate the interlocking block resistance to sliding. The proposed method allows equating an interlocking block to a conventional block with different sliding resistances along two orthogonal directions (normal and parallel to the connectors).
2. The goal of the second stage is to present a new structural analysis procedure that, applying the heuristic method proposed above, checks if the semi-circular arches composed of interlocking blocks are stable. To achieve this goal, this work extends the limit analysis developed by [16] which applied the line of thrust method to analyze the stability of semi-circular arches composed of blocks with *isotropic finite friction*. The extension deals with semi-circular arches composed of interlocking blocks which, using the heuristic method, are modelled as conventional blocks with *orthotropic finite friction* (in which the sliding resistances are the minimum and maximum in two orthogonal directions, respectively), in order to analyze their structural stability.
3. Finally, the third stage of this research is to develop an optimization method minimizing the structurally feasible semi-circular arch thickness. The structural feasibility of the model during optimization is checked by the introduced structural analysis procedure.

Considering the relationship between the block resistance to sliding and the geometry of interlocking faces, the optimization method offers two strategies to minimize the arch thickness: (1) updating the sliding resistance due to the connector geometry change during optimization; (2) changing the number of the block connectors (initially given by the designer) during the optimization process, to keep the sliding resistant constant.

The paper is organized as follows. The structural modelling along with the heuristic method introduced above are presented in Section 2, while Section 3 performs the extension of limit state analysis to interlocking blocks. Section 4 develops two optimization strategies to design semi-circular arches with interlocking blocks. Results are presented, discussed and validated in Section 5. Finally, the conclusions are summarized in Section 6.

2. DISCRETE MODEL FOR THE SEMI-CIRCULAR ARCH COMPOSED OF INTERLOCKING BLOCKS

2.1. Structural model of the interlocking block arch

The structural model adopted in this work is based on the assumption that masonry structures are composed of assemblages of discrete rigid interlocking blocks in contact interaction, to be constitutively defined, where the displacements of each block should be considered separately. How a semi-circular arch and each of its discrete interlocking blocks are modelled in the developed framework is described as follows.

Within the arch modelling, the designer assigns the radius R for the semi-circular arch centreline, the arch width b, and the number of blocks m composing the arch (Figure 1a). The latter number should be odd to model the arch keystone. All arch blocks have same sizes.

On the other hand, the block modelling is based on the assumption that each interlocking block has two corrugated and two flat faces. Interlocking faces lock blocks to form the arch and the corrugated faces of the connectors are assumed to have rectangular cross sections (Figure 1b). Different shapes of the connectors could be investigated, but this further analysis will be addressed in future work. To model the interlocking faces, the designer should specify the total number n of projections and depressions of the block. This number should be an odd number in order to guarantee the symmetry of the block shape with respect to the centreline of the arch.

Within the introduced discrete approach, the block interfaces are treated as the elements of the problem while the blocks are simply defining the geometry of the problem. Therefore, the analysis is fully related to the behaviour of the interfaces, which can then be regarded as

systems of stresses. Considering conventional blocks with rough flat faces in contact with finite friction, these stresses are governed by unilateral contacts and isotropic frictional constraints, due to the rugged projections on their faces, termed asperities. By scaling up the asperities, they can be regarded as connectors of two interlocked blocks.

Using corrugated interlocking faces, the block resistance to sliding at the interface is a minimum along the connectors and a maximum along the direction normal to the connectors (Figure 1b). In fact, the friction on the equivalent flat face can be regarded as orthotropic friction, in which the sliding resistances are the minimum and maximum in two orthogonal directions, respectively. The next section presents a method to analyse the sliding resistance of an interlocking block and to relate the sliding resistance of interlocking blocks to the frictional resistance of conventional blocks.

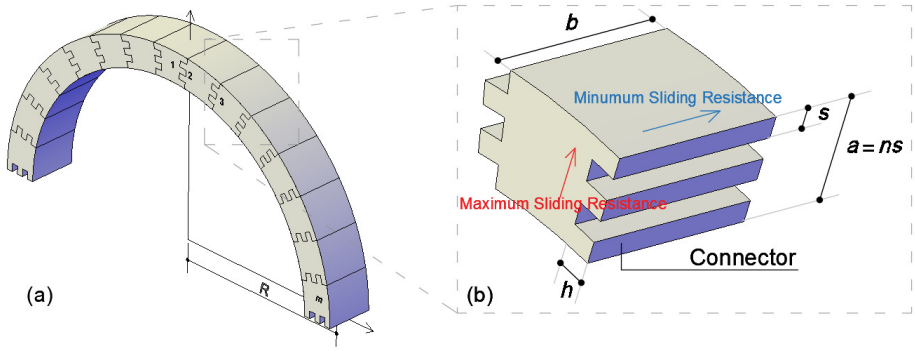

Figure 1. Topological models of a) a semi-circular arch and b) a composing interlocking block.

2.2. Heuristic formulations relating the sliding resistance of interlocking blocks to the frictional resistance of conventional blocks

The interlocking blocks could have different sliding resistances in different directions, depending on the orientation and the mechanical and geometrical features of the connectors. For example, the interlocking block adopted in this work has the maximum and minimum sliding resistance respectively along the direction normal and parallel to the connectors. This section is aimed at defining a heuristic relationship between the sliding resistance of such interlocking blocks and that of the equivalent conventional blocks with rough flat interfaces. Finding such a relationship, limit state analysis method is then extended to analyse the structural behaviour of a semi-circular arch composed of interlocking blocks (Section 3).

The first step for searching out this relation is to study the sliding resistance along the direction orthogonal to the connectors of interlocking blocks. The analysis is carried out with reference to a single interface between a fixed lower block and the upper one subjected to a given normal force N and a lateral load T applied to its centre of gravity (Figure 2a). In order

to consider the same sliding resistance for two interlocking blocks, depressions and projections have the same width s, so that $a = ns$, being n an odd number with $n \geq 3$.

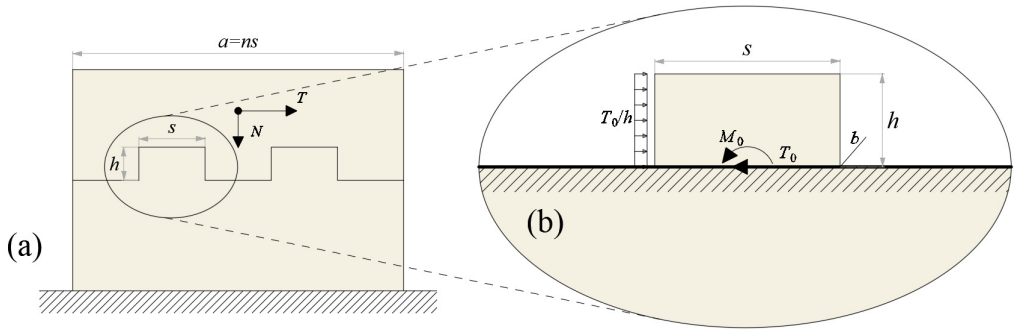

Figure 2. Geometric parameters of the interlocking blocks and their projections. a) Upper block subjected to lateral force T and its own weights; b) limiting shear force and bending moment of the single projection.

The assumptions for interlocking blocks are: infinite compressive strength, frictional behaviour at the bed joints, finite shear and tensile strengths of the connectors. The sliding failure mode essentially behaves in a rigid perfectly-plastic manner as for conventional blocks when it is governed by the frictional resistances [34, 35], while it is non-ductile when governed by the shear strength. With these assumptions, the lateral resistance of this block at first step is strictly related to the shear and/or bending resistances of the connectors and at second step, after the connector shear or bending failures, it is related to the cracked block frictional resistance.

In this paper the moment failure mode of projections is prevented, though. The exclusion of the bending failure can be derived in terms of geometrical relation between the width s and the height h of the projections, with reference to the simplest case of uniformly distributed horizontal forces sketched in Figure 2b. In fact, in order to avoid the bending failure before the shear failure of the single projection, it should be thick enough, i.e.:

$$h \leq s \tag{1}$$

This constraint is derived by the following assumptions. The limiting shear force and bending moment activating the corresponding failure modes of the single projection can respectively be expressed in function of the connector dimensions as obtained by using the classical Jourawski and Navier formulas [36]:

$$T_0 = \frac{2}{3}\tau_k sb \qquad M_0 = f_{tk}\frac{bs^2}{6} \tag{2}$$

where τ_k and f_{tk} are the shear and tensile strengths of the material forming the blocks, respectively. The calibration of parameter τ_k is not generally provided within the mechanical properties of the material and it should be experimentally defined. However, for the sake of simplicity and conservative results, by assuming as a first approximation that $\tau_k = 0.5\, f_{tk}$ (as in case of pure shear and according to the Tresca yield criterion [37]), Eq. (1) is derived from the condition to prevent moment failure that is $T_0 < T'_0$, where T'_0 is the shear corresponding to the limiting moment M_0 ($T'_0 = 2M_0/h$).

On the other hand, to analyze how the frictional and shear resistances interact with each other, three different models have been considered: a model including interlocking blocks with similar heights of connectors (Figure 3) and two models including different heights of the lower and upper connectors (Figures 4 and 5). In the first model, due to the simultaneity of the bed contacts between each projection and depression, each connector is subjected to shear and compressive forces. On the other side, in the second and third models in Figures 4 and 5, respectively, the connectors of one block are subjected to shear and compressive forces, while the connectors of the other block are only subjected to shear forces. The shear resistance of a connector which is subjected to shear and compressive forces T''_0 is greater than the shear resistance of a connector which is only subjected to pure shear forces T_0, because of the effect of the compression. This means that the weaker connectors are the latter ones and as a result, this paper aims at considering T_0 as the ultimate shear forces a connector can resist (the more conservative choice).

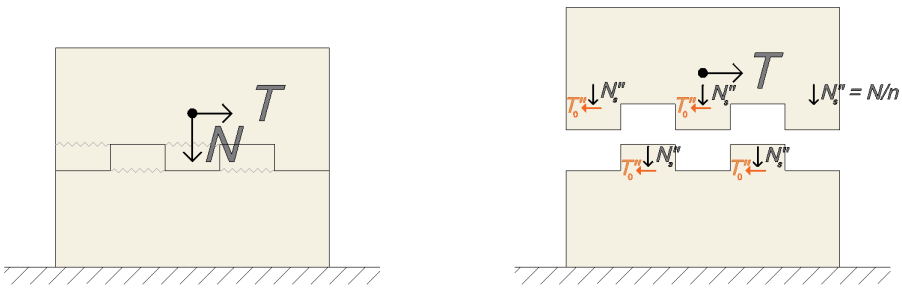

Figure 3. Sliding resistances of interlocking blocks with same height for two-block connectors (Case 1).

The resultant sliding resistance of the interlocking blocks can be derived both with reference to Cases 2 and 3. In both cases, the frictional resistances (T_s and T'_s in Figures 4 and 5) may activate only after the shear collapse of the connectors on bed joints represented by the thicker blue lines in the figures.

Therefore, considering Case 2 (Figure 4), where the upper projections are higher than the lower ones, the bed joints of the two interlocking blocks are localized at the bottom

depressions of the lower block. In this case, the shear resistances of each upper and lower block connector are T''_0 and T_0, respectively. Whatever the position of projections i) or ii) in Figure 4, the resultant limiting shear force of all connectors and the frictional resistance of all bed joints respectively are:

$$T_R = \frac{n-1}{2} T_0; \qquad T_C = N\mu \tag{3}$$

where μ is the friction coefficient, N is the fixed normal force (including the own weight of the upper block).

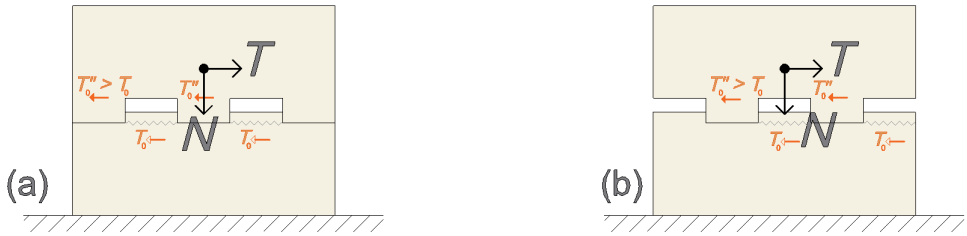

Figure 4. Sliding resistances of interlocking blocks with upper connectors higher than lower ones (Case 2).

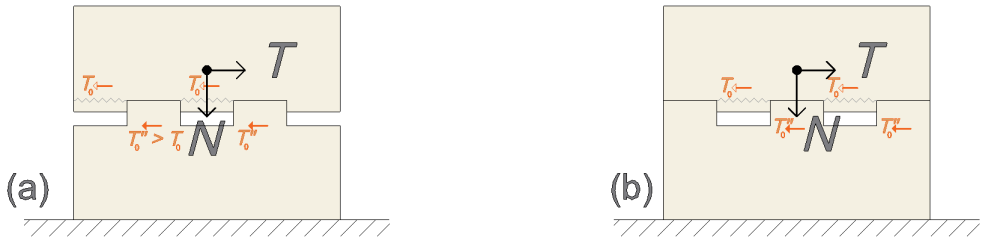

Figure 5. Sliding resistances of interlocking blocks with lower connectors higher than upper ones (Case 3).

Since the failure mode is first governed by the shear collapse of the projections, the ultimate lateral force strongly depends on the amounts of the two resistances of Eq. (3). In fact, if $T_R > T_C$ the ultimate lateral force will be $T = T_R$ because once the failure is activated the frictional resistance is not enough to prevent sliding. This condition, implying non-ductile behaviour of the interface, is represented by the black dot in Figure 6a, where the greater constant shear resistance is superposed on the choesionless Coulomb yield condition. On the contrary, if $T_R < T_C$ the lateral force will be governed by T_C ($T = T_C$) and a ductile behaviour may occur because at the onset of the shear failure mode of projections the frictional resistances will also be activated and the sliding is prevented until the shear achieves the value T_C (Figure 5b).

This means that, to avoid sliding of an interlocking block in the direction normal to the connectors, the following inequality should be always met:

$$T \leq \max(\mu N, T_R) \tag{4}$$

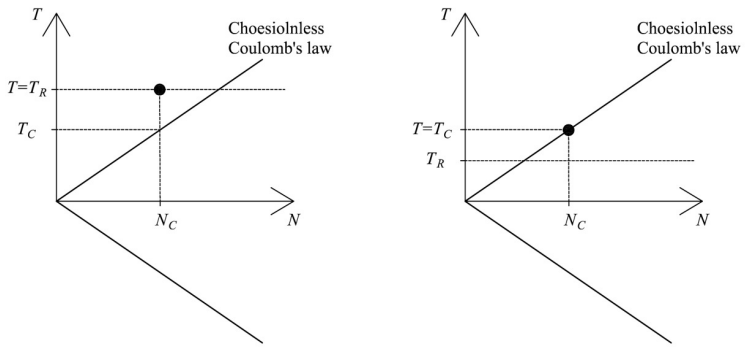

(a) (b)

Figure 6. Ultimate lateral force in the a) non-ductile case $T_R > T_C$ and b) ductile case $T_R < T_C$.

Using the first expression of Eq. (2), Ineq. (4) can be rewritten as:

$$T \leq \max\left(\mu N, \left(\frac{n-1}{3n}\right)\tau_k ab\right) \tag{5}$$

which represents the relationship between the geometries of the projections and interlocking block sliding resistance, limited by being *n* an integer and odd number. This inequality also shows that the sliding resistance depends on either friction coefficient or shear strength of the block.

On the other hand, if Case 3 is considered (Figure 5), the bed joints of the two interlocking blocks are localized at the top projections of the lower block. In this case, the shear resistances of each lower and upper block connector are T''_0 and T_0, respectively. In fact, it is easy to verify within Figure 5 that the positions of projections i) and ii) for Case 3 are the mirrored positions ii) and i) for Case 2, respectively, about a horizontal line. Therefore, as in Case 2, the lateral resistance is governed by the relationship between the two resistances (Figure 6) and the geometrical parameters satisfying Ineq. (5).

Besides, the sliding in the direction parallel to the connectors is only governed by the inequality $T \leq \mu N$. This means that the interlocking block proposed by this paper can be considered as a conventional block with orthotropic friction so that the frictional constraints are Ineq. (5) or $T \leq \mu N$, depending on the direction.

The heuristic formulation given by Ineq. (5) will be applied in the next section to the limit state analysis of a semi-circular arch composed of interlocking blocks and subjected to its own weight. In this case, only the sliding resistance along the direction orthogonal to the

connectors of interlocking blocks is activated. Later in Section 4, this heuristic formulation will be implemented to develop the optimization algorithm for such structures.

3. LIMIT ANALYSIS OF A SEMI-CIRCULAR ARCH COMPOSED OF INTERLOCKING BLOCKS

As introduced in Section 1, standard limit analysis of rigid block assemblages has been found to be a valuable computational tool for developing two groups of structural optimization problems: 1) to find the maximum load a structure can tolerate (predict the collapse load); and 2) to find the minimum material (i.e., minimum thickness) a structure can have to bear a specific amount of load. Both approaches lead to find the classical rocking failure mechanism of such structures.

To develop these optimization problems, either static or kinematic theorems can be applied. The occurrence of Coulomb frictional sliding, which implies non-associative flow rule, is in general excluded from the analysis in order to ensure the validity of the normality condition, one basic hypothesis of classic limit state analysis. In fact, it is well-known that the bounding theorems of plastic limit analysis do not in general provide unique solutions for the collapse load factor if a non-associative flow rule is specified [34] and the classical procedure does not assure that the structure is safe.

However, Casapulla and Lauro [16] have identified a special class of non-associative friction problems for which provably unique solutions exist. The class comprises arches with symmetrical loading and geometry. The proposed procedure was applied to arches of this sort to both verify that the numerical and analytical solutions coincide and to investigate the convergence characteristics of the method.

Exploiting the uniqueness of the solution due to the symmetry, the present work is mainly aimed at extending this optimization method to design the minimum thickness of a semi-circular arch composed of interlocking blocks and subjected to its own weight.

In fact, to minimize the thickness of such an arch, first the desired radius for the arch centreline R is specified and then the optimization problem tries to find the closest thrust line to this centreline which satisfies the equilibrium and yield conditions at contact interfaces.

This section explains how to find a thrust line meeting equilibrium and yield conditions. Next section introduces two optimization strategies to find the optimal conditions.

The general thrust line is defined by a set of control points variable in function of two points A(0; Y_A) and B(X_B; 0), respectively at the crown and the springing joints (Figure 7a). The X-

coordinates of the control points are the same of the application points of each block weight, while the Y-coordinates are found as follows. Given X_B and Y_A, the horizontal reactive thrust H_{tot} can be found as:

$$H_{tot} = W_{tot} \frac{X_B - X_W}{Y_A} \tag{7}$$

where W_{tot} is the weight of the half-arch and X_w is the X-coordinate of the half-arch centre of mass. Being W_i the weight of block i and x_i^t the X-coordinate both of its application point and of the control point i, ΔY_i can be achieved by applying the equilibrium condition:

$$\Delta Y_i = \frac{\Delta X_i \sum_{i=1}^{i-1} W_i}{H_{tot}} \tag{8}$$

where $\Delta X_i = {x_{i+1}}^t - x_i^t$. Knowing ΔY_i, Y-coordinate of control point i, can be achieved by:

$$y_i^t = y_{i+1}^t + \Delta Y_i \tag{9}$$

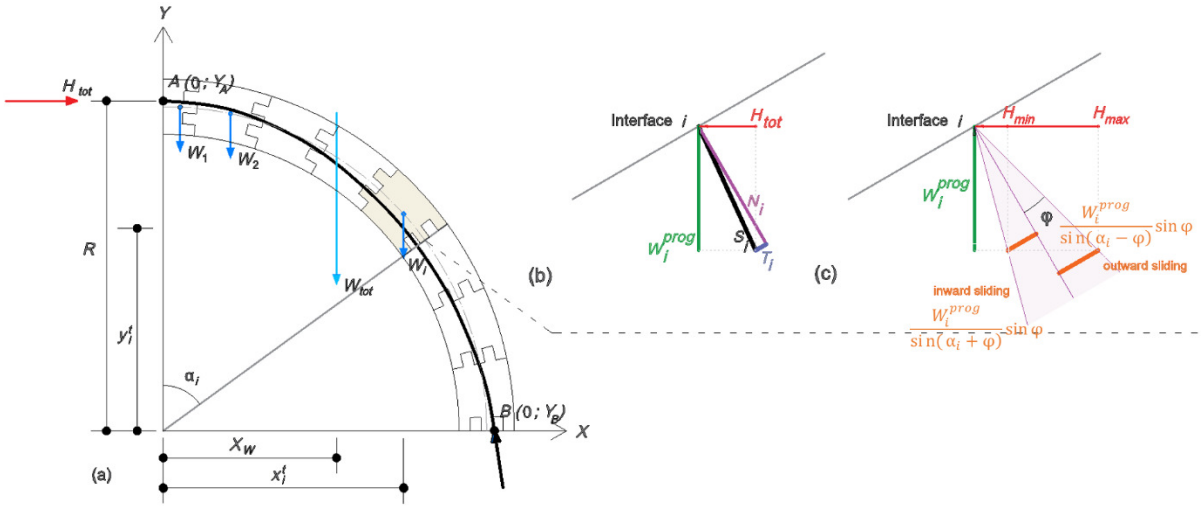

Figure 7. Thrust line in the half interlocking block arch.

A valid thrust line should also meet the yield conditions at contact interfaces. Applying the heuristic method described in Section 2.2, interlocking blocks composing a semi-circular arch can be considered as conventional blocks whose sliding resistance can be evaluated by Ineq. (5) which for interface i can be rewritten as:

$$T_i \leq \max\left(N_i \tan(\varphi), \left(\frac{n-1}{3n}\right) \tau_k a b\right) \tag{10}$$

where T_i and N_i are the tangential and normal components of S_i, respectively, (Figure 7b) and $\tan(\varphi)$ equals μ. According to Casapulla and Lauro's method [16], for the case of semi-circular arch subjected to symmetric loads, the ultimate value for T_i is independent of N_i and

the expression $N_i \tan(\varphi)$ can be substituted by two expressions $\frac{W_i^{prog}}{\sin(\alpha_i+\varphi)} \sin\varphi$, for inward T_i and $\frac{W_i^{prog}}{\sin(\alpha_i-\varphi)} \sin\varphi$, for outward T_i (Figure 7c); where W_i^{prog} is the sum of weights form blocks 0 to i and α_i is the angle between the lower contact joint of the block i and Y-axis.

After this substitution, Ineq. (10) can be splitted into the two following yield conditions for semi-circular arches composed of interlocking blocks:

$$|T_i| \leq \max\left(\left(\frac{W_i^{prog}}{\sin(\alpha_i+\varphi)} \sin\varphi\right), \left(\left(\frac{n-1}{3n}\right)\tau_k ab\right)\right) \quad \text{inward } T_i \tag{11}$$

$$|T_i| \leq \max\left(\left(\frac{W_i^{prog}}{\sin(\alpha_i-\varphi)} \sin\varphi\right), \left(\left(\frac{n-1}{3n}\right)\tau_k ab\right)\right) \quad \text{outward } T_i \tag{12}$$

Lastly, it should be taken into consideration that since all block weights, the thrust line, and the limiting sliding forces for all blocks lie on the same plane, the problem can be considered as a 2d problem. In this case, the sliding resistance of all interfaces with orthotropic friction is only regarded to be the maximum sliding resistance value on those interfaces (orthogonal to the connectors in Fig. 1b). This means that an arch with interlocking blocks which embeds a thrust line whose control points are obtained by Eqs. (7) and (9) and meets Ineqs. (11) and (12), is a stable arch.

4. STRUCTURAL OPTIMIZATION

As explained earlier, the optimization problem of this paper is aimed at finding the closest thrust line to the specified arch centreline (minimum thickness) which satisfies the equilibrium and yield conditions at interfaces.

Unlike the conventional blocks whose frictional properties remain fixed during optimization, changing the arch thickness during optimization may change the sliding resistance at interfaces. In the following sub-sections, two strategies are proposed to minimize the arch thickness (Figure 8), based on different relationships between the geometry of the interlocking interfaces and the sliding resistance. In the first strategy, the sliding resistance changes during the optimization process; in the second strategy, the geometric properties of interfaces changes in a way that the sliding resistance remains fixed during optimization.

For both strategies the objective function is the minimization of the maximum value of the arch half-thickness ($a_{\min}/2$), as described in [16] for the arch with conventional blocks. The variables of the problem are X_B and Y_A of the generic thrust line (Figure 7).

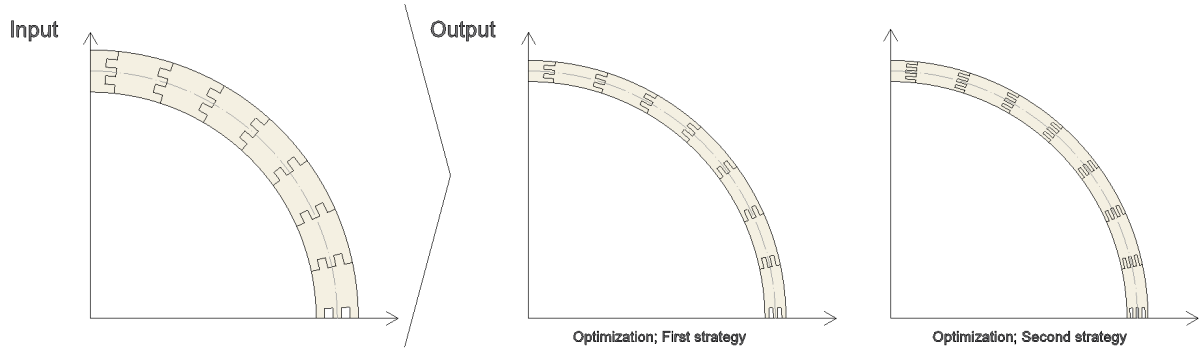

Figure 8. Two optimization strategies to minimize the thickness of a semi-circular arch with interlocking blocks.

4.1. First strategy

In this strategy, the number of projections and depressions n at each interface remains fixed during the optimization. As a result, changing the arch thickness a during optimization, the shear resistance of interfaces changes as well.

The thrust line should also meet the yield conditions by satisfying Ineqs. (11) and (12) during the optimization. Hence, the optimization problem for this strategy is as follows:

$$\textbf{Min max } \max\left(\sqrt{(x_i^t)^2 + (y_i^t)^2} - R\right) \tag{13}$$

S.T.

$$|T_i| \leq \max\left(\left(\frac{W_i^{prog}}{\sin(\alpha_i+\varphi)}\sin\varphi\right), \left(\frac{n-1}{3n}\right)\tau_k b 2 \max\left(\sqrt{(x_i^t)^2 + (y_i^t)^2} - R\right)\right) \quad \text{inward } T_i$$

$$|T_i| \leq \max\left(\left(\frac{W_i^{prog}}{\sin(\alpha_i-\varphi)}\sin\varphi\right), \left(\frac{n-1}{3n}\right)\tau_k b 2 \max\left(\sqrt{(x_i^t)^2 + (y_i^t)^2} - R\right)\right) \quad \text{outward } T_i$$

The optimal arch only embeds the obtained thrust line and transforms the statically indeterminate structure into a mechanism with hinges and/or sliding surfaces, as described in Section 5.

4.2. Second strategy

In this strategy, shear resistance T_R remains fixed during optimization via changing the number of the connectors. Given the initial values for X_B and Y_A (X_B^0 and Y_A^0), the initial Y-coordinates of the control points (y_i^{t0} for block i) and then the fixed T_R^0 can be obtained. In fact, given the initial n (n^0) which should be at least three, and considering the arch initial half-thickness ($a_0/2$) to be the maximum distance between the radius and control points on this thrust line, the initial value of shear resistance T_R^0 can be calculated as follows:

$$T_R^0 = \left(\frac{n_0-1}{3n_0}\right)\tau_k b 2\max\left|\sqrt{\left(x_i^{t0}\right)^2+\left(y_i^{t0}\right)^2}-R\right| \quad (14)$$

where x_i^{t0} is the same as x_i^t of the objective function (13).

This value remains fixed during optimization, while both arch thickness a and n change during optimization. Given n^0, x_i^{t0} and y_i^{t0}, the relation between a (which equals $2\left|\sqrt{(x_i^t)^2+(y_i^t)^2}-R\right|$) and n can be defined as follows:

$$n = \frac{n_0.(2\max)}{n_0.\left(2\max\left|\sqrt{\left(x_i^t\right)^2+\left(y_i^t\right)^2}-R\right|\right)+\left(2\max\left|\sqrt{\left(x_i^t\right)^2+\left(y_i^t\right)^2}-R\right|\right)(1-n_0)} \quad (15)$$

which should be an (a) integer, (b) odd, and (c) positive number during optimization. As a result, the optimization problem for the second strategy is as follows:

$$\textbf{Min } \max\left|\sqrt{(x_i^t)^2+(y_i^t)^2}-R\right| \quad (16)$$

S.T.

$$|T_i| \le \max\left(\left(\frac{W_i^{prog}}{\sin(\alpha_i+\varphi)}\sin\varphi\right), T_R^0\right) \qquad \text{inward } T_i$$

$$|T_i| \le \max\left(\left(\frac{W_i^{prog}}{\sin(\alpha_i-\varphi)}\sin\varphi\right), T_R^0\right) \qquad \text{outward } T_i$$

$$n = \lfloor n \rfloor;\ n\%2 = 1;\ n \ge 0$$

This objective function of the optimization problem is the same as the previous strategy and the sliding resistance of the arch is met by applying the two first inequalities.

5. RESULTS AND EVALUATIONS

This section is composed of two main parts. First, a case study of a semi-circular arch of 10m centreline radius, containing 27 discrete blocks is analyzed by means of the two introduced optimization strategies. These results are investigated to compare the two proposed optimization strategies to each other and to the Casapulla and Lauro's optimization method developed for arches with conventional blocks [16]. Then, to evaluate the accuracy of the proposed heuristic method and the limit state analysis method, the interlocking block interface and the case study are analysed by Finite Element method for comparison.

5.1. Case study

In the following, after a brief description on the implemented process, the case study is presented to investigate the relation between the minimum arch thickness, obtained by the two introduced optimization strategies, and the sliding resistance of the block interfaces. Finding these relations, minimum thickness/Radius (t/R) ratio can be defined as a function of the parameters determining the block sliding resistance.

5.1.1. Implementation

For modelling the arch with its interlocking blocks and also for part of the structural calculations, Grasshopper's C# component was applied. Grasshopper is a visual programming language which runs within Rhinoceros 3D. Another part of the structural calculations and optimization are performed by MATLAB used as backend. For the optimization, MATLAB's fminimax method was used. Multiple hard constraints in the second strategy imposed on variable *n* could have led to find no solution. To avoid this, soft constraints were used, weighted through trial and error to achieve the most reliable results.

5.1.2. Optimal arches with conventional blocks

This sub-section uses the results obtained by Casapulla and Lauro's optimization method for the sake of comparison with the results obtained by the proposed optimization strategies applied to conventional blocks. Figure 9 shows the relationship between the predicted minimum arch thickness required for stability and the coefficient of friction for the introduced semi-circular arch with conventional blocks.

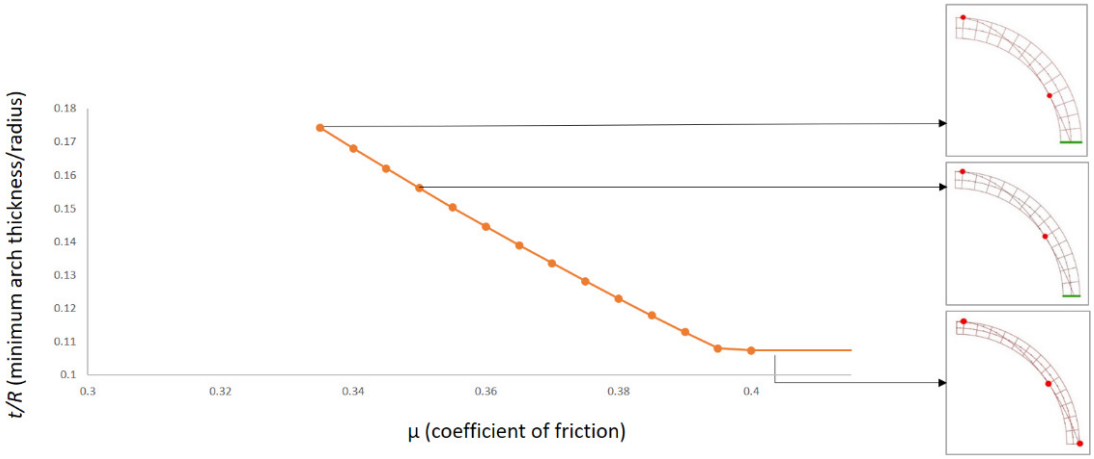

Figure 9. Relationship between the minimum thickness of an arch composed of conventional blocks and the coefficient of friction; red points show formed hinges and green lines represent block sliding interfaces.

It results that: 1) for $\mu > 0.395$, the Heyman's theoretical minimum thickness of 10.7% of the centreline radius is approximately reproduced with this discretization (10.74%) and the failure mode is governed by a pattern of hinges at the intrados and extrados; 2) for $0.395 \geq \mu \geq 0.332$, the failure mechanism is characterized by the sliding interfaces at the horizontal supports along with hinges at the crown and at variable points in between; 3) for $\mu < 0.332$ the equilibrium is no longer possible.

5.1.3. Optimal arches with interlocking blocks obtained by the first optimization strategy

Figure 10 shows the relationship between the predicted minimum arch thickness required for stability and the friction coefficient for the introduced arch composed of interlocking blocks with fixed $n = 5$. This relationship varies for different values of parameter $\frac{T_R^f}{T_U}$, where T_R^f is shear resistance obtained by the first of Eq. (3) for a_{min} and T_U is the ultimate frictional resistance of an interface at the onset of the sliding failure. Therefore, when $\frac{T_R^f}{T_U} \leq 1$, the frictional resistance is greater than the shear resistance and when $\frac{T_R^f}{T_U} \geq 1$ it is vice versa.

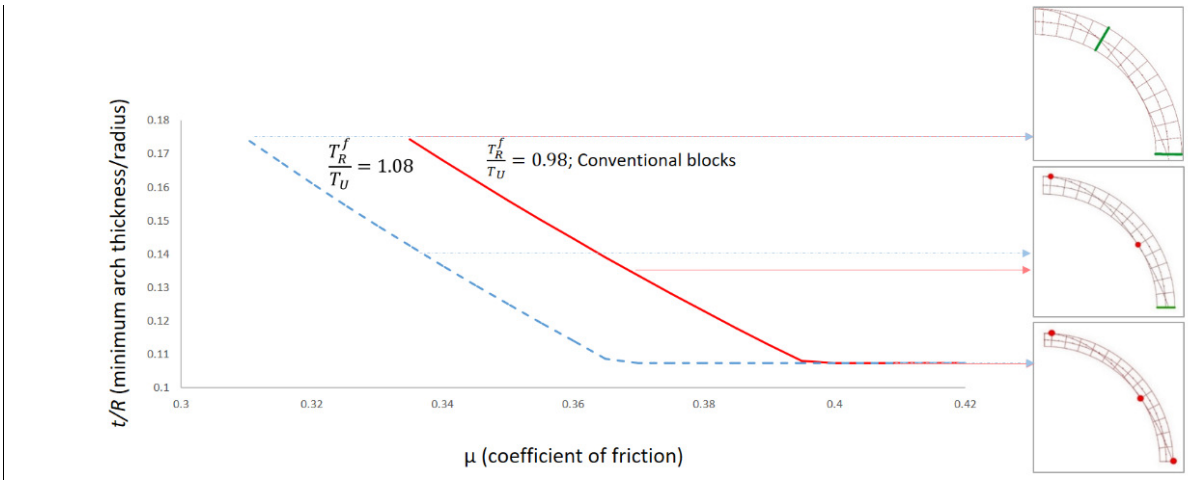

Figure 10. Relationship between the minimum thickness of an arch composed of interlocking blocks and the coefficient of friction- 1st optimization strategy; red circles show formed hinges and green lines represent block sliding interfaces.

Figure 10 represents both the case of $\frac{T_R^f}{T_U} = 0.98$, in which the arch behaves as an arch with conventional blocks and the case of $\frac{T_R^f}{T_U} = 1.08$, whose curve is horizontally moved to the left side. As shown in the figure, the minimum friction coefficient assuring stability has a lower

value compared to the minimum one for an arch with conventional blocks, since T_R and not T_U determines the arch sliding resistance. This result is consistent with the discussion provided in Section 2.2 on the heuristic formulations.

The results obtained from the first strategy can also be represented from a larger perspective by Figure 11, for μ between 0.3 and 0.4 and $\frac{T_R^f}{T_U}$ between 0.98 and 1.20.

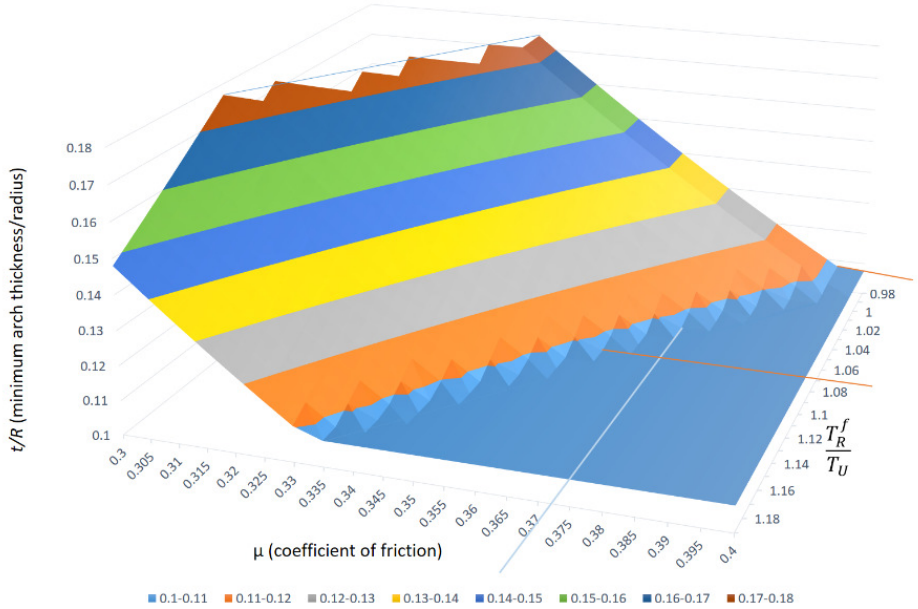

Figure 11. Relationship between the minimum thickness of an arch composed of interlocking blocks, the coefficient of friction, and $\frac{T_R^f}{T_U}$- 1st optimization strategy.

Any section of this figure along the direction of μ-axis, presents the relation between the minimum arch thickness required for stability and $\frac{T_R^f}{T_U}$. For example, Figure 12 shows a section of the graph in Figure 11, corresponding to $\mu = 0.37$. According to this graph when $\frac{T_R^f}{T_U}$ is smaller than one (the frictional resistance is greater than the shear resistance), the minimum arch thickness is equal to the minimum thickness of an arch composed of conventional blocks with $\mu = 0.37$. When $\frac{T_R^f}{T_U}$ is larger than 1.07, the sliding resistance is large enough so that hinges form earlier than sliding failure. In this case, the minimum arch thickness is equal to the minimum thickness of an arch composed of conventional blocks with $\mu > 0.395$.

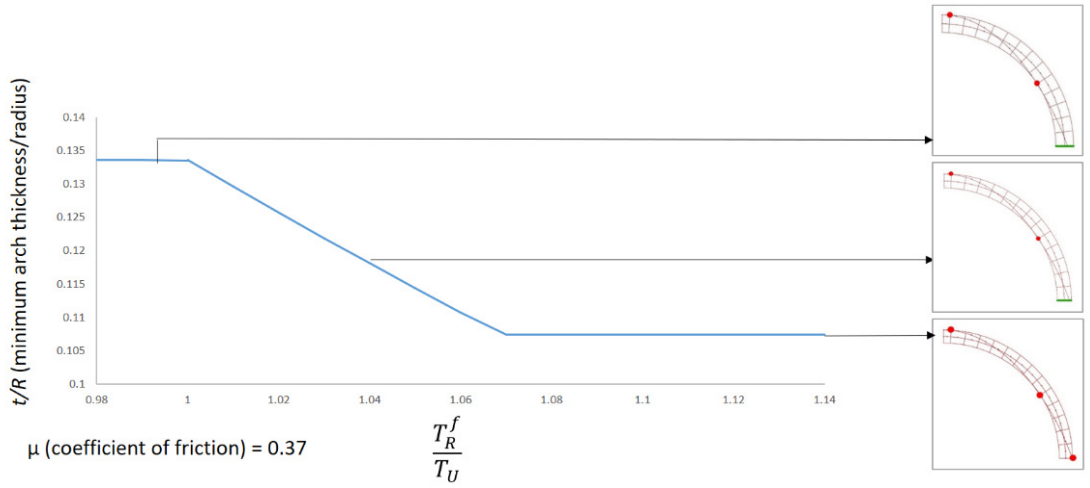

Figure 12. Relationship between the minimum thickness of an arch composed of interlocking blocks and $\frac{T_R^f}{T_U}$- 1st optimization strategy; red circles show formed hinges and green lines represent block sliding failure.

5.1.4. Optimal arches with interlocking blocks obtained by the second optimization strategy

According to the second strategy proposed above, the initial value of the shear resistance is fixed while the arch thickness and the number of connectors change during optimization.

First, it is worth highlighting that the final result (a_{min}) is highly dependent on the initial values of the optimization parameters (Y_A^0, X_B^0), due to the way that the final n is related to Y_A^0 and X_B^0, i.e.:

$$n = \frac{a_{min}\, n_0}{a_{min}\, n_0 + a_0(1-n_0)} \tag{17}$$

In fact, Eq. (17) is obtained when the initial value of shear resistance T_R^0, which should remain fixed during optimization, is calculated according to Eq. (14). Considering the final n to be a positive value in Eq. (17), this inequality should be always met:

$$a_{min}\, n_0 \geq a_0(n_0 - 1) \tag{18}$$

and this means that the final result a_{min} is dependent on the initial thickness a_0 which is determined by Y_A^0 and X_B^0.

Secondly, it should also be underscored that the minimum thickness obtained by the second strategy might differ from that of the first strategy for the same values of friction coefficient and $\frac{T_R^0}{T_U}$ in order to guarantee that T_R^0 is kept unchanged during the optimization of the second strategy, i.e. that it is:

$$a_{min}\, \frac{n-1}{n} = a_0\, \frac{n_0-1}{n_0} \tag{19}$$

The right hand side of this equation is a known value while a_{min} and n should be chosen so that this value is achieved. Both a_{min} and n are constrained variables; a_{min} should satisfy the equilibrium condition with sliding constraints and n should be a positive odd value. As a result, a_{min} satisfying Eq. (19) might be different from results of first optimization strategy.

It is concluded that the thrust line which is found as the optimal result may not be the unique solution of the arch embedding it. In other words, the rocking failure mechanism of the arches cannot be precisely found. Still, the closest possible solution to that failure mechanism can be found as follows.

For example, Figure 13 depicts the tangential force at interface m of the case study optimized by the first strategy when this interface reaches the limiting sliding value (blue curve). This figure also depicts the tangential force at interface m of the case study (${X_B}^0$ and ${Y_A}^0$ equal 10.81 m) optimized by the second strategy (red curve) for the same $\frac{T_R^0}{T_U}$. As shown, these two curves are quite close but not identical. In fact, blue curve represent the closest possible value to the limiting one satisfying Eq. (17)

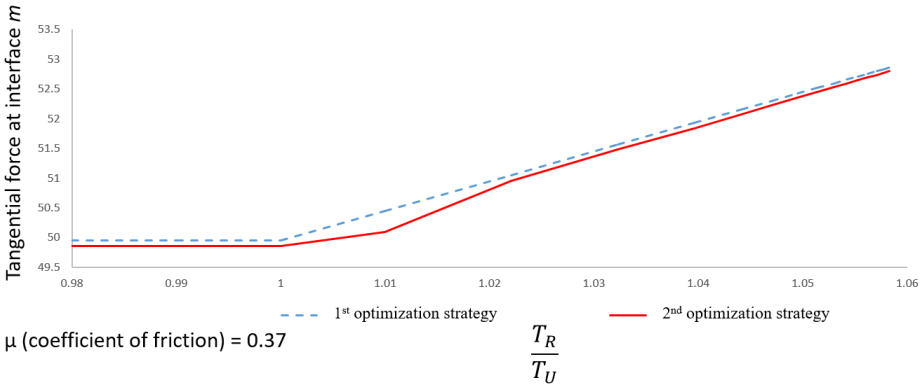

Figure 13. Difference between tangential force at interface m for the optimal arch optimized by first and second optimization strategies

Build on the two discussed issues, the relationship between the minimum arch thickness required for stability and $\frac{T_R^0}{T_U}$ for the arch explained above, with $n_0 = 3$ and ${X_B}^0$ and ${Y_A}^0$ equal to 10.81 m, is as follows (Figure 14- yellow continuous curve). When $\frac{T_R^0}{T_U}$ is smaller than 1.01, the minimum arch thickness equals 1.36 m. It is worth noting that for $1 \leq \frac{T_R^0}{T_U^B} \leq 1.01$ there is no set of a_{min} smaller than 1.36 m and n by which Eq. (19) is satisfied. When $\frac{T_R^0}{T_U}$ is larger than 1.06, the minimum arch thickness equals 1.12 m. According to Ineq. (17), a_{min} should be

greater than 1.09. The closest a_{min} to this limiting value which satisfies Eq. (19) is calculated to be 1.12 m.

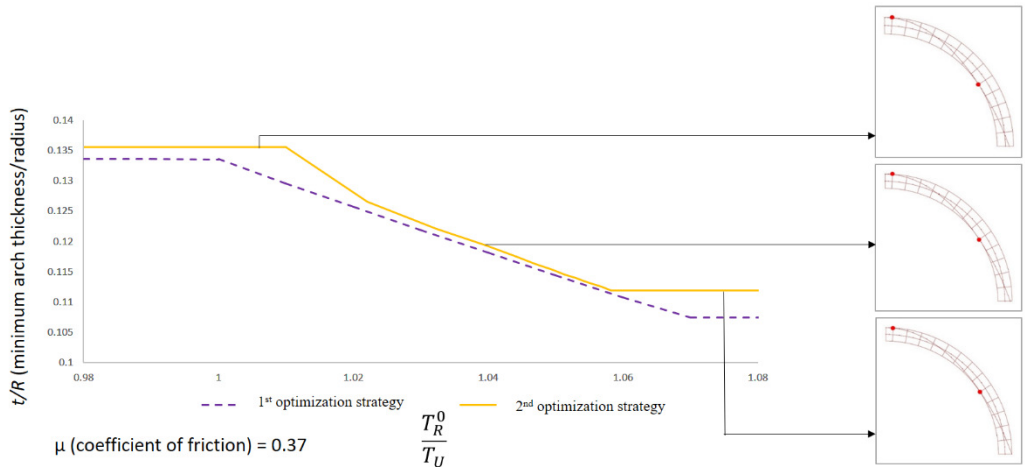

Figure 14. Relationship between the predicted minimum thickness of an arch composed of interlocking blocks and $\frac{T_R^0}{T_U}$- 2nd optimization strategy; red circles show formed hinges.

Satisfying both Ineq. (17) and Eq. (19), yellow continuous curve in Figure 14 is slightly different from that of Figure 12 (results of the first strategy) which is redisplayed by purple dash curve. Still, their overall configuration is similar, as explained above.

Figure 15 shows the relationship between the final n for the optimal arch and $\frac{T_R^0}{T_U}$. According to this graph, for $\frac{T_R^0}{T_U}$ greater than 1.0583, the final n remains fixed while all interfaces are resistant enough against sliding so that failure occurs due to the hinge formation. The graph also shows that increasing $\frac{T_R^0}{T_U}$ the rate of change of final n increases.

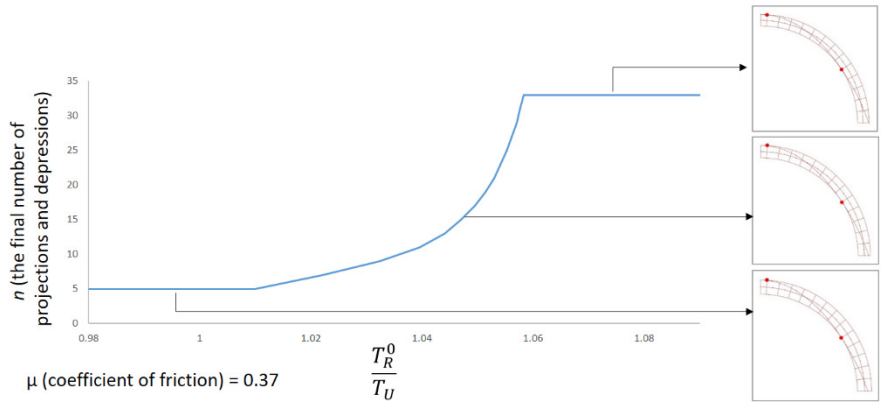

Figure 15. Relationship between the final number of projections and depressions n for the optimal arch composed of interlocking blocks and $\frac{T_R^0}{T_U}$- 2nd optimization strategy; red circles show formed hinges.

5.2. Validation and calibration via FEA

The heuristic method and the extension of limit analysis of this paper are validated by comparing the results obtained by the proposed methods with the results achieved by Finite Element Analysis (FEA) based on the simplified macro modelling technique proposed by [32]. In this method, blocks are morphed (controlled expansion) to eliminate mortar joints and are considered to be solid or shell elements, while mortar joints are zero-thickness interface elements. This validation includes three parts: in the two first parts the proposed heuristic method is studied by analysing two sets of interlocking blocks with different geometries; the third part studies the proposed limit analysis methods and optimization strategies by analysing the case study of the arch analysed above.

The FEA is developed in ABAQUS 6.11-1 by adopting the brittle cracking model. In the first two parts, to purely focus on the shear behaviour at the joint between the main body and the connectors of a block, the following model is designed and analysed: two stacked blocks with a shared interlocking interface are modelled. The connectors and the main body of each of the blocks are modelled with rigid body elements (rigid parts) while the joint between them is modelled with C3D8R elements (flexible part with brittle behaviour) (Figures 16b and 18b). The material properties of elements are shown in Tables 1. The effective density of the expanded blocks is calculated using homogenization process proposed in [32].

Table 1. Material properties of expanded blocks.

Compressive strength	4.14	MPa
Tensile Strength	0.36	MPa
Shear strength	0.5 f_{tk}= 0.18	MPa
Effective Young's modulus	3	GPa
Poisson's ratio	0.25	
Effective density	$\rho = \frac{(150 \times 0.5 \times 0.24) - (340 \times 0.5 \times 0.01)}{0.5 \times 0.25} = 130.4$	Kg/m^3
Block density	150	Kg/m^3
Mortar density	340	Kg/m^3

The lower face of the lower block is bounded so that no degree of freedom is allowed. The upper face of the upper block is bounded so that one degree of freedom is allowed in the direction of lateral force application. The loads imposed on the model are the weight of the upper block and a lateral force distributed on a vertical face of this block (Figures 16c and 18c). The lateral force by which the principal stress reaches the tensile strength is found. This value is compared to the shear resistance obtained by the proposed heuristic method. The distribution of principal stresses and shear stresses τ_{xy} in X direction on the plane whose

normal vector is *Y* is studied as well. The elastic analysis is used to find the stress state of the model.

5.2.1. Analysis of interlocking blocks with $n = 3$

Figure 16a shows the size of the blocks in meters and the layout of rigid and flexible parts of each block.

The maximum lateral force obtained by FEA is 9.42 kN, when the maximum principal stress (0.36 MPa) is observed on the joint between the connector and main body of the lower block.

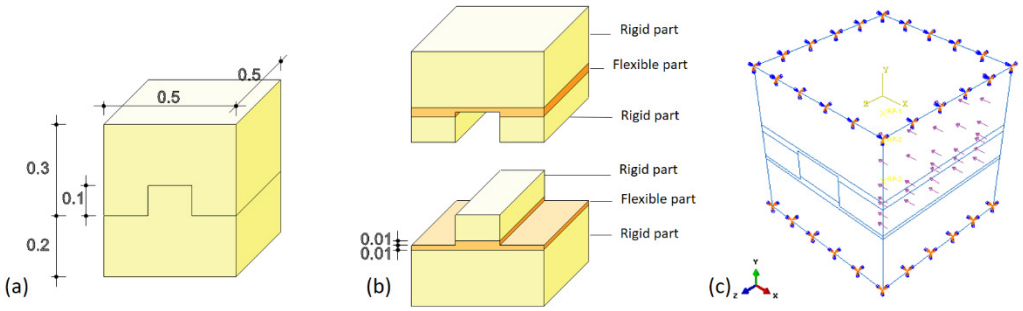

Figure 16. a) Dimensions of the analysed model with $n = 3$; b) layout of rigid and flexible elements; c) boundary conditions and lateral force distributed on the upper block.

The maximum τ_{xy} is also 0.177 MPa. Figure 17 presents the distribution of principal stresses and τ_{xy} on the connector of the lower block which is maximum at two edges of the connector (τ_{xy} are 0.177 and 0.134 MPa) and minimum in the middle of connector (τ_{xy} is 0.122 Mpa).

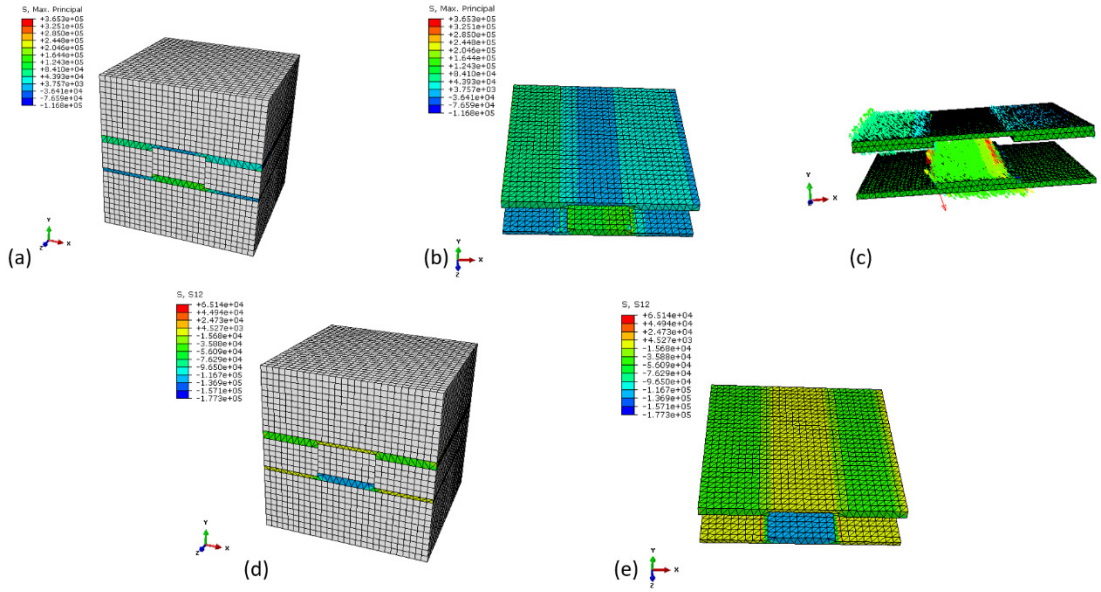

Figure 17. Principal stress state for a) the whole model with $n = 3$ and b) for the two flexible layers of the two blocks; c) directions of the principal stresses; d) τ_{xy} for the whole model and e) at the two flexible layers of the two blocks.

Using Eq. (3), the sliding resistance of the proposed heuristic method is calculated: $2/3 \times 0.18 \times 10^3 \times 0.167 \times 0.5 = 10.02$ kN. The ratio of sliding resistance obtained by FEA to the proposed heuristic method is 0.94, showing a very good agreement between these results.

5.2.2. Analysis of interlocking blocks with $n = 7$

Figure 18 presents the size of the blocks in meters and the layout of rigid and flexible parts of each block.

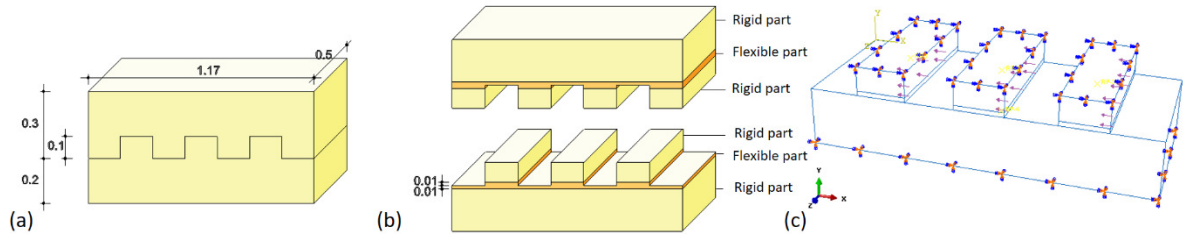

Figure 18. a) dimensions of the analysed model with n=7; b) layout of rigid and flexible elements; c) boundary condition, the distributed lateral force is imposed on the upper block vertical face in *–X direction.*

The maximum lateral force obtained by FEA is 26.1 kN. As shown in Figure 19, the maximum principal stress (0.36 MPa) is observed on the joint between the main body of the lower block and the connector that is closer to the lateral face where the horizontal load is applied. The maximum τ_{xy} of 0.201 MPa occurs on the same joint. However, the stresses are not uniformly distributed on all the three joints between the three connectors and the main body of the lower block. The more a joint is closer to the applied lateral force, the larger stresses it has. For lateral force of 26.1 kN, the maximum principal stresses on joints between each of the two further connectors and the main body of the lower block are 0.3 and 0.276 MPa. This means that, depending on the interaction between the other connectors after the failure of the first connector, the final value of the force that corresponds to the failure of all the connectors would be larger than 26.1 kN.

The sliding resistance according to the heuristic method (Eq. 3) equals $3 \times 2/3 \times 0.18 \times 10^3 \times 0.167 \times 0.5 = 30.06$ kN. This value is slightly larger than that obtained by FEA because of the failure of all the connectors. Actually, this difference between the maximum force obtained by FEA and the heuristic method could be due to the difference of the lateral force application point. In the heuristic method, in fact, this point is considered to be the centroid of the upper block and, consequently, the stresses are uniformly distributed on all the joints between the connectors and the main body of the block.

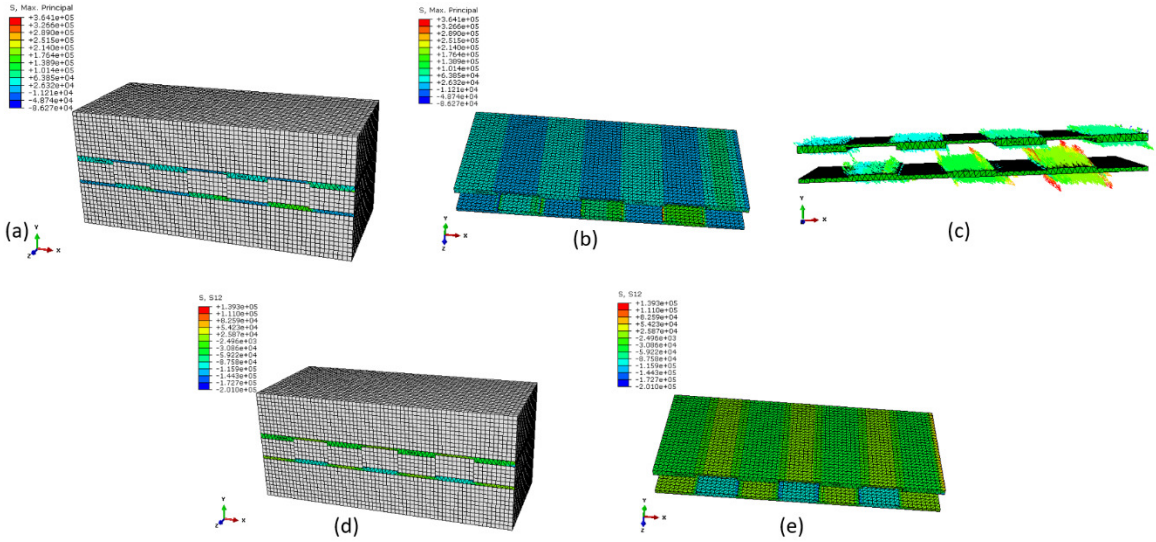

Figure 19. Principal stress state for a) the whole model with $n = 7$ and b) for the two flexible layers of the two blocks; c) directions of the principal stresses; d) τ_{xy} for the whole model and e) at the two flexible layers of the two blocks.

5.2.3. Analysis of the case study arch composed of interlocking blocks with $n = 5$

In the case of the arch with assigned radius $R = 10$m and subjected to its own weight, blocks are modelled with C3D8R elements and the mortar joints between them are modelled as shell interfaces with friction coefficient $\mu = 0.37$. The material properties are those reported in Table 1, with the exception of the Young's modulus which is increased to 6 GPa. The modelling of rigid body elements used in the previous analyses is no longer suitable to the case of the arch due to the presence of non-negligible bending moments at interfaces. This implies some limits of validation for the proposed heuristic method which is based on the pure shear condition. However, the validation of the optimal arch with thickness of 1.07 m, obtained by the first optimization procedure for $\frac{T_R^f}{T_U} = 1.08$, is herein performed, mainly in terms of failure mode.

In fact, using the proposed limit state method, for this optimal model the pure rocking mechanism is observed, that is fully captured by the FE model, as shown in Figure 20.

In sum, the three cases examined in this section can be considered a good validation of the proposed heuristic method and optimization procedure, with some limitations in the case of rocking/sliding failure modes. Further studies and experimental investigation will be provided by future work.

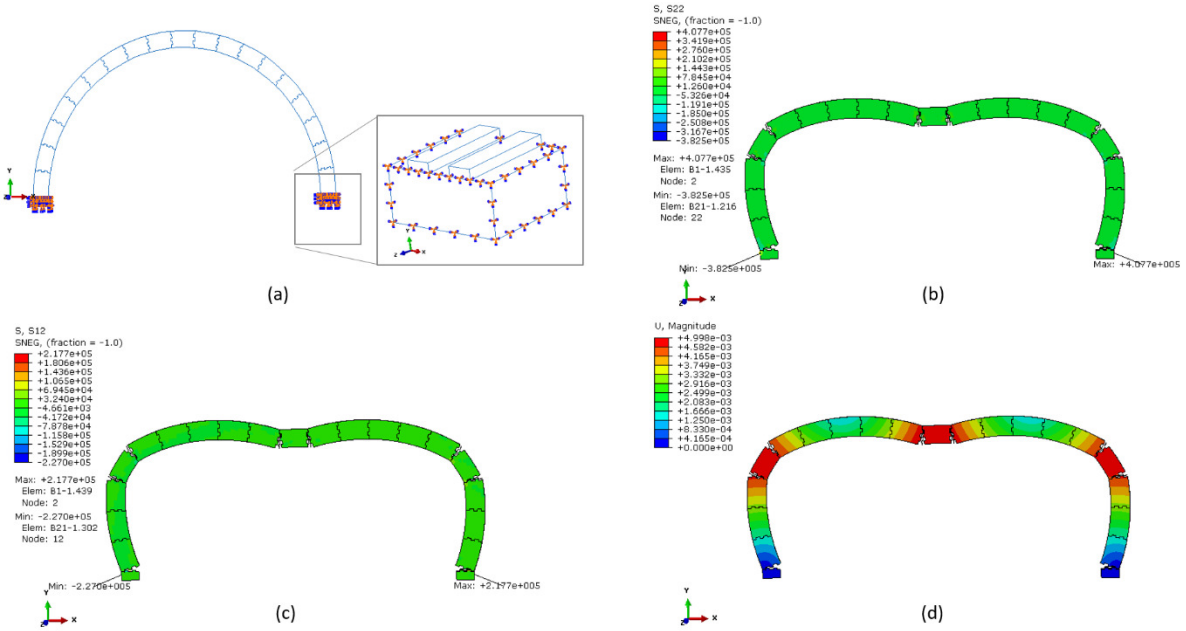

Figure 20. a) boundary condition; b) normal stresses in Y direction (σ_y); c) shear stresses in X direction on a plane whose normal vector is Y (τ_{xy}); d) deformation of the arch $\frac{T_R^f}{T_U} = 1.08$.

6. CONCLUSIONS

A Digital tool was developed to design the structurally sound semi-circular arch with interlocking blocks. The main achievements of this research are:

• a heuristic method to find the relationship between the geometric properties of the interlocking connectors and the block sliding resistance;

• a limit state analysis approach to analyze the stability of arches composed of interlocking blocks; by using the heuristic method, it extends the limit state approach in order to define a new stability condition for semi-circular arches composed of interlocking blocks when the interface sliding resistance varies in different directions;

• two optimization methods to minimize the thickness of the semi-circular arches composed of interlocking blocks via adjusting the control points of constructed the thrust line for the arch; this work extends the optimization algorithm finding the thinnest structurally feasible arch composed of blocks with finite friction. In this extension the newly developed condition of stability (sliding constraint) for arches composed of interlocking blocks are applied. In the first method, the sliding resistance changes during the optimization. The results show that if the shear resistance is less than the frictional resistance, the arch behaves as an arch with conventional blocks. When the shear resistance is larger than the frictional resistance, the

structural behaviour of the arch is governed by the shear strength. For small values of shear strength, the combined rocking/sliding mechanism occurs for the optimal result. For large values of shear strength, pure rocking mechanism can be observed on the optimal result.

In the second method, the sliding resistance is kept fixed via changing the number of the connectors. The results are mostly dependent on the constraints keeping the number of the connectors an odd integer value and also on the initial value of sliding resistance defined by the designer. Due to these items, the optimal result for the minimum thickness might be thicker comparing to the result of the first optimization method, given the same shear strength, friction coefficient and geometric inputs. In this case, the mechanism does not occur on the optimal solution.

A good agreement of the results obtained by the heuristic method and optimization procedure was found in case of pure shear conditions, while some limits of validation were highlighted in case of mixed rocking/sliding failure modes. Future works will address these issues together with the extension of the approach to the 3d models. Furthermore, the sliding resistance of interlocking blocks will also be experimentally investigated together with the analysis of different shapes of the interfaces.

ACKNOWLEDGMENTS

 This project has received funding from the European Union's Horizon 2020 research and innovation programme under the Marie Skłodowska-Curie Grant Agreement No. 791235. It reflects only the authors' view and the Agency is not responsible for any use that may be made of the information it contains.

References

[1] Dyskin, A.V., Pasternak, E. Estrin, Y. (2012). Mortarless structures based on topological interlocking. Frontiers of Structural and Civil Engineering, 6(2): 188-197.

[2] Ramamurthy, K., Kunhanandan Nambiar, E.K. (2004). Accelerated masonry construction review and future prospects. Progress in Structural Engineering and Materials, 6(1): 1-9.

[3] Rippmann, M. (2016). Funicular Shell Design: Geometric approaches to form finding and fabrication of discrete funicular structures. Ph.D. thesis, ETH-Zürich, Zürich.

[4] Whiting, E.J.W. (2012). Design of structurally-sound masonry buildings using 3d static analysis. Ph.D. thesis, MIT, Massachusetts.

[5] Brocato, M., Mondardini, L. (2012). A new type of stone dome based on Abeille's bond. International Journal of Solids and Structures, 49(13): 1786-1801.

[6] Kanel-Belov, A.Y., Dyskin, A.V., Estrin, Y., Pasternak, E., Ivanov-Pogodaev, I.Y.A.E. (2010). Interlocking of convex polyhedra: towards a geometric theory of fragmented solids. Moscow Mathematical Journal, 10(2): 337-342.

[7] Heyman, J. (1966). The stone skeleton. International Journal of solids and structures, 2(2): 249-279.

[8] Livesley, R.K. (1978). Limit analysis of structures formed from rigid blocks. International Journal for Numerical Methods in Engineering, 12(12): 1853-1871.

[9] Livesley, R.K. (1992). A computational model for the limit analysis of three-dimensional masonry structures. Meccanica 27(3): 161-172.

[10] Gilbert, M., Casapulla, C., Ahmed, H.M. (2006). Limit analysis of masonry block structures with non-associative frictional joints using linear programming. Computers and structures, 84(13): 873-887.

[11] Casapulla, C., Maione, A., Argiento, L.U., Speranza, E. (2018). Corner failure in masonry buildings: an updated macro-modeling approach with frictional resistances. European Journal of Mechanics - A/Solids, 70: 213-225.

[12] Casapulla, C., Argiento, L.U. (2018). In-plane frictional resistances in dry block masonry walls and rocking-sliding failure modes revisited and experimentally validated. Composites Part B: Engineering, 132: 197-213.

[13] Casapulla, C., Argiento, L.U. (2016). The comparative role of friction in local out-of-plane mechanisms of masonry buildings. Pushover analysis and experimental investigation. Engineering Structures, 126: 158-173.

[14] Hawksbee, S., Smith, C., Gilbert, M. (2013). Application of discontinuity layout optimization to three-dimensional plasticity problems. Proc. R. Soc. A, 469(2155), 20130009.

[15] Harvey, W. J. (1988). Application of the mechanism analysis to masonry arches. Structural Engineer 66(5): 77–84.

[16] Casapulla, C., Lauro, F. (2000). A simple computation tool for the limit-state analysis of masonry arches. In Proceedings of the 5th International Congress on Restoration of Architectural Heritage (Firenze 2000), Firenze (Italy), pp. 2056-2064.

[17] D'Ayala, D., Casapulla, C. (2001). Limit state analysis of hemispherical domes with finite friction. In Proceedings of the 3rd International Conference on Structural Analysis of Historical Constructions (SAHC01), Guimaraes (Portugal), pp.617-626.

[18] D'Ayala, D.F., Tomasoni, E. (2011). Three-dimensional analysis of masonry vaults using limit state analysis with finite friction. International Journal of Architectural Heritage, 5(2): 140-171.

[19] O'Dwyer. D.W. (1999). Funicular analysis of masonry vaults. Computers and Structures, 73(1-5): 187-197.

[20] Block, P., Ochsendorf, J. (2007). Thrust network analysis: A new methodology for three-dimensional equilibrium. Journal-International Association for Shell and Spatial Structures, 155: 167-173.

[21] Casapulla, C., Maione, A. (2016). Formulating the Torsion Strength of Dry-Stacked Stone Blocks by Comparing Convex and Concave Contact Formulations and Experimental Results. Indian Journal of Science and Technology, 9(46): 1-7.

[22] Beatini, V, Royer-Carfagni, G., Tasora, A. (2018). The role of frictional contact of constituent blocks on the stability of masonry domes. Proc. R. Soc. A 474: 20170740.

[23] Cavalagli, N., Gusella, V., Severini L. (2016). Lateral loads carrying capacity and minimum thickness of circular and pointed masonry arches. International Journal of Mechanical Sciences, 115: 645-656.

[24] Misseri, G., DeJong, M.J., Rovero, L. (2018). Experimental and numerical investigation of the collapse of pointed masonry arches under quasi-static horizontal loading. Engineering Structures, 173: 180-190.

[25] Ye, C., Acikgoz, S., Pendrigh, S., Riley, E., DeJong, M.J (2018). Mapping deformations and inferring movements of masonry arch bridges using point cloud data. Engineering Structures,173: 530-545.

[26] Di Carlo, F., Coccia, S., Rinaldi, Z. (2018). Collapse load of a masonry arch after actual displacements of the supports. Archive of Applied Mechanics, 88: 1545-1558.

[27] Galassi, S. Misseri, G., Rovero L., Tempesta G. (2018). Failure modes prediction of masonry voussoir arches on moving supports. Engineering Structures, 173: 706-717.

[28] Owen, D.R.J., Peric, D., Petrinic, N., Brookes, C.L., James, P.J. (1998). Finite/discrete element models for assessment and repair of masonry structures. Proc. II Int. Arch Bridge Conf. on "Arch Bridges–History, analysis, assessment, maintenance and repair", Venice (Italy), AA Balkema.

[29] Bui, T.T., Limam, A., Sarhosis, V., Hjiaj, M. (2017). Discrete element modelling of the in plane and out of plane behaviour of dry joint masonry wall constructions. Engineering Structures, 136: 277-294.

[30] Forgács, T., Sarhosis, V., Bagi, K. (2018). Influence of construction method on the load bearing capacity of skew masonry arches. Engineering Structures, 168: 612-627.

[31] Lourenco, P.B., Rots, J.G., Blaauwendraad, J. (1995). Two approaches for the analysis of masonry structures: micro and macro-modeling. HERON, 40(4): 1995.

[32] Li, T., Atamturktur, S. (2013). Fidelity and robustness of detailed micromodeling, simplified micromodeling, and macromodeling techniques for a masonry dome. Journal of Performance of Constructed Facilities, 28(3): 480-490.

[33] Milani, E., Milani, G., Tralli, A. (2008). Limit analysis of masonry vaults by means of curved shell finite elements and homogenization. International Journal of Solids and Structures, 45(20): 5258-5288.

[34] Kooharian, A. (1952). Limit analysis of voussoir (segmental) and concrete arches. Journal of American Concrete Institute, 24(4): 317-28.

[35] Drucker, D.C. (1954). Coulomb friction, plasticity and limit loads. Journal of Applied Mechanics, 21(1): 71-4.

[36] Timoshenko, S.P., Goodier, J.C. (1970). Theory of Elasticity. McGraw–Hill Co. Inc., New York.

[37] Dowling, N.E. (1998). Mechanical behavior of materials. 2nd edition, Prentice-Hall, Englewood Cliffs, New Jersey.